International Journal of Nanoelectronics and Materials
*Volume 16, No. 3, July 2023* [511-522]

# Comparative Study and Modeling of AlGaN/GaN Heterostructure HEMT and MOSHEMT Biosensors

Abdellah Bouguenna[1*], Driss Bouguenna[2], Amine Boudghene Stambouli[1] and Aasif Mohammad Bhat[3]

[1]Electrical Engineering Laboratory of Oran, Department of Electronics, Faculty of Electrical Engineering, University of Sciences & Technology of Oran (USTO-MB), 31000, Oran, Algeria
[2]Geomatics, Ecology and Environment Laboratory, Nature and Life Sciences Faculty, and ST Department, Mascara University, 29000, Mascara, Algeria
[3]Department of Electronics and Communication Engineering, Malaviya National Institute of Technology, 302017 Jaipur, India

Received 10 August 2022, Revised 20 November 2022, Accepted 28 November 2022

**ABSTRACT**

*This paper presents a comprehensive comparative study and analytical modelling of electrical performance of AlGaN/GaN high-electron-mobility transistor (HEMT) and metal-oxide-semiconductor high-electron-mobility transistor (MOSHEMT) biosensors. Sensing parameters such as the I-V characteristics and sensitivity parameter for biomolecules detection in the cavity region are taken into consideration. In this paper, the permittivity is varied according to the biomolecule to be sensed by the biosensor. The maximal variation of the electrical performance of the biosensor obtained is higher in HEMT as compared with MOSHEMT. The simulation results of the analytical model obtained by using MATLAB verified by a comparison with experimental data and atlas-technology computer aided design (Atlas-TCAD), and shown good agreement with each other. Thereby, we could improve the validity of the proposed model. The AlGaN/GaN HEMT have shown good sensing of 141.73 at biomolecular permittivity of 2.5 which can be used for biosensing applications effectively.*

**Keywords:** AlGaN/GaN, Biosensors, HEMT, MOSHEMT, Permittivity.

## 1. INTRODUCTION

Biosensors are analytical devices use chemical reactions to detect the biological chemistry compounds such as biomolecules, antibodies, nucleic acids, enzymes etc . The wide bandgap semiconductors like gallium nitride (GaN) have excellent physical properties which gives them an important position for many applications. The GaN devices can operate at high power, high frequency and high temperature compared to Silicon [1]. One of the most important applications of GaN is in the field of biosensors as AlGaN/GaN high-electron-mobility transistors (HEMTs) exhibit good biocompatibility, stable material properties and high sensitivity to the sheet density charge since the two-dimensional electron gas (2DEG) in the channel is well close to the surface [2], which is order of $10^{13}$ $cm^{-2}$ [3]. The charges in the channel of AlGaN/GaN HEMTs are induced by spontaneous and piezoelectric polarisation, which are balanced with positive charges on the surface [4]. An oxide layer such as $Al_2O_3$ [5], is inserted between gate metal and barrier layer which results in metal oxide semiconductor high-electron-mobility transistors (MOSHEMTs) [3, 6, 7]. The surface charges at the AlGaN/GaN heterointerface varies by the specific biomolecules which can get easily attached to AlGaN barrier layer and as a counter effect channel property are varied [1]. Extensive studies have been conducted on AlGaN/GaN HEMT to detect different biomolecules such as protein [8], $Hg^{2+}$ [9], DNA [10],

* Corresponding author: abdellah.bouguenna@univ-usto.dz

ammonium ions and urea [11], c-erbB-2 [12], Ebola Antigen [13], SARS-CoV-2 [14] and as well as pH [15]. Various structures are also optimized like Circular gate HEMT, Double gate, Gate-less devices, Nano-cavity under the gate region towards the drain side, and Nano-cavity at the source and drain both sides to enhance the sensitivity of the proposed HEMTs device [16].
Aasif et al use $Al_2O_3$ passivation that ensures uniform oxide surface (sensing membrane), low defect density, chemically stable characteristics, high electrical insulation in GaN/AlN/AlGaN MOSHEMT based biosensor [17].

In this paper, AlGaN/GaN HEMT is designed to operate as biosensors and is compared with MOSHEMT by immobilizing the biomolecules in the cavity region this comparison presents the effect of oxide material on performance of biosensors. We have simulated the output and the transfer characteristics, the transconductance and sensitivity parameter of AlGaN/GaN HEMT and MOSHEMT for protein biomolecule detection and compare the electrical performance of both devices for biosensing applications.

Besides, this paper is organised as follows: the AlGaN/GaN HEMT and MOSHEMT device structures and conduction band profile are presented in the section 2. The section 3 derives the expressions of the analytical model for the electrical properties have been also presented. In the results and discussion section, the numerical simulation results of the model analytical of electrical characteristics of GaN based AlGaN/GaN HEMT and MOSHEMT obtained by MATLAB are presented and compared with necessary simulation results extracted by Atlas-TCAD, which have proved the validity of the analytical model. Finally, the conclusion is drawn in section 5.

## 2. AlGaN/GaN HEMT & MOSHEMT STRUCTURES AND CONDUCTION BAND PROFILE

Figure 1 shows the cross section of AlGaN/GaN HEMT and MOSHEMT devices. From top to bottom the layers are grown as follows: metal/AlGaN/GaN case of HEMT and metal/$Al_2O_3$/AlGaN/GaN case of MOSHEMT with a 2-DEG formed at the AlGaN/GaN heterointerface. GaN buffer layer is grown on $Al_2O_3$ substrate. Besides, the Figure 2 present the conduction energy band diagram of HEMT and MOSHEMT based on AlGaN/GaN heterostructures.

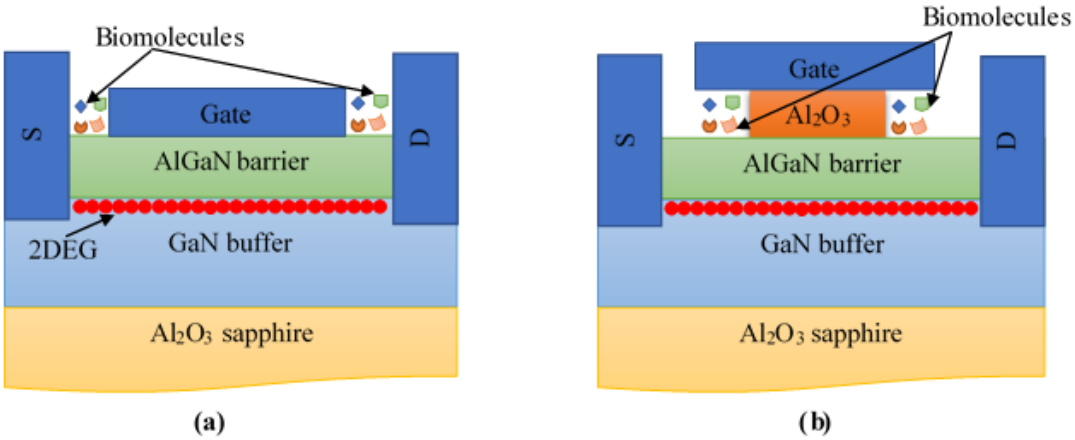


**Figure 1.** Structures of the AlGaN/GaN biosensors. (a) HEMT and (b) MOSHEMT.

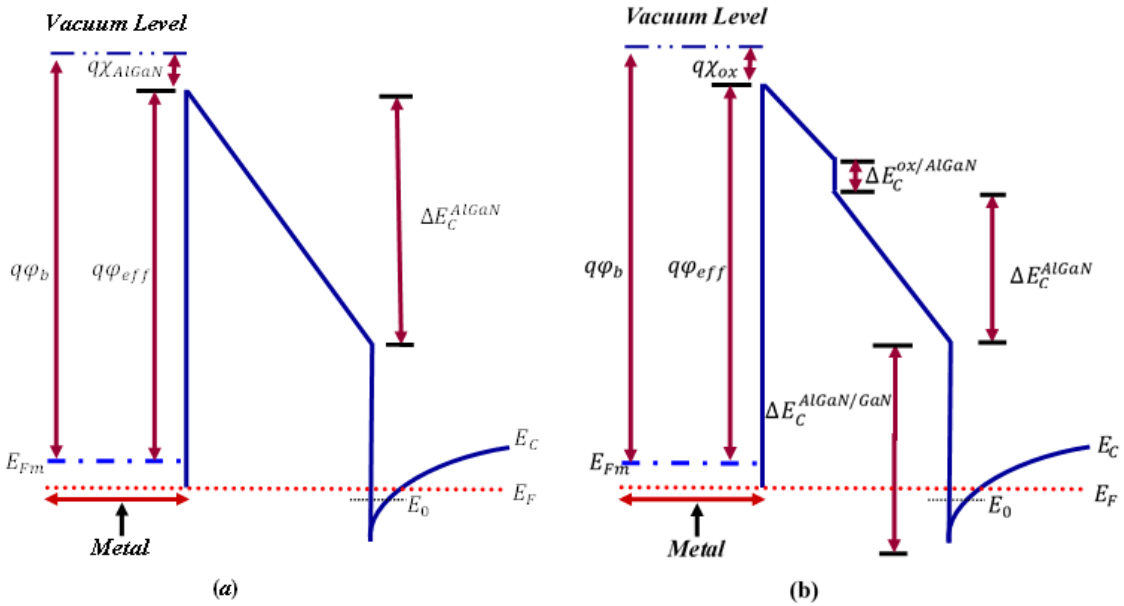


**Figure 2.** Conduction energy band profiles of AlGaN/GaN heterostructures. (a) HEMT (b) MOSHEMT.

## 3. ANALYTICAL MODEL FOR THE ELECTRICAL PROPERTIES

### *3.1 Model of the threshold voltage for AlGaN/GaN heterostructures based HEMT and MOSHEMT*

The threshold voltage of the AlGaN/GaN heterostructures based HEMT and MOSHEMT device can be derived when the device is completely off and the 2-DEG is pinched-off. Under this condition, the difference between level the minimum energy of an electron in 2-DEG and the energy of the Fermi reduces to zero, so $n_s$ and $E_F$ become zero. setting done these two conditions and substituting $\emptyset_s$ by $(\emptyset_{s(air)} - V_{gs})$ into Eq. (1) [18].
Where $\emptyset_{s(air)}$ is the surface potential at zero gate potential and $V_{gs}$ is the applied gate voltage.

The sheet charge concentration can be written as

$$n_s = \sigma_{pol}/q - (\varepsilon_{AlGaN}/q^2(d_{AlGaN} + t_{ox})[q\emptyset_s + E_F(n_s) - \Delta E_c] \quad (1)$$

where $\emptyset_{s(air)}$ is given by Eq. (2) [18]

$$\emptyset_{s(air)} = \gamma_{air}(\emptyset_M - \chi_{AlGaN}) + (1 - \gamma_{air})\emptyset_0 - \frac{\gamma_{air} q N_D d_{AlGaN}}{C_{eff(air)}} \quad (2)$$

The threshold voltage is expressed as

$$V_{th1} = \gamma_{air}(\emptyset_M - \chi_{AlGaN} + (1 - \gamma_{air})\emptyset_0 - \gamma_{air}\frac{qN_D d_{AlGaN}}{C_{eff(air)}} - \Delta E_c - \frac{\sigma_{pol} q d_{AlGaN}}{k_{AlGaN}} \quad (3)$$

After introducing the biomolecules in the cavity region, the surface potential can be written as [18]

$$\emptyset_{s(bio)} = \gamma_{bio}(\emptyset_M - \chi_{AlGaN}) + (1 - \gamma_{bio})\emptyset_0 - \frac{\gamma_{bio} q N_f d_{AlGaN}}{C_{eff(bio)}} \quad (4)$$

where $\gamma_{air} = \frac{1}{1+D_{it}\,q^2/C_{eff(air)}}$ and $N_D$ is the doping concentration of AlGaN barrier layer and $\gamma_{bio} = \frac{1}{1+D_{it}\,q^2/C_{eff(bio)}}$ and $N_f$ represents the biomolecules charge density. The threshold voltage for both devices HEMT and MOSHEMT without and with biomolecules can be written as

$$V_{th2} = \gamma_{bio}(\emptyset_M - \chi_{AlGaN} + (1-\gamma_{bio})\emptyset_0 - \gamma_{bio}\frac{qN_{Df}d_{AlGaN}}{C_{eff(bio)}} - \Delta E_c - \frac{\sigma_{pol}qd_{AlGaN}}{k_{AlGaN}} \quad (5)$$

where $C_{eff(air)} = (2C_{air} + C_{ox}) \times C_b/(2C_{air} + C_{ox} + C_b)$ and $C_{eff(bio)} = (2C_{bio} + C_{ox}) \times C_b/(2C_{bio} + C_{ox} + C_b)$ are the effective capacitances without and with biomolecules for MOSHEMT, respectively.
$C_{eff(air)} = (2C_{air}) \times C_b/(2C_{air} + C_b)$ and $C_{eff(bio)} = (2C_{bio}) \times C_b/(2C_{bio} + C_b)$ are the effective capacitances without and with biomolecules for HEMT, respectively.

$C_{bio} = \varepsilon_{bio}/d_{bio}$ is the capacitance of the cavity region, $\varepsilon_{bio}$ is the biomolecule permittivity and $d_{bio}$ is the biomolecule thickness. $C_{ox} = \varepsilon_{ox}/d_{ox}$ and $t_{ox}$ represent the capacitance and thickness of the oxide layer, respectively. $C_b = \varepsilon_{AlGaN}/d_{AlGaN}$ represents the capacitance AlGaN layer.

Where $q$ and $\sigma_{pol}$ represent the electronic charge and the polarisation induced charge density at the AlGaN/GaN heterointerface, respectively. $E_F$ is Fermi level position and $\varepsilon_{AlGaN}$ is the dielectric permittivity of barrier lager AlGaN as a function of the Al mole fraction, is given by [18]

$$\varepsilon_{AlGaN} = 9.5 - 0.5x \quad (6)$$

Electron affinity of AlGaN is written as

$$\chi_{AlGaN} = \chi_{GaN} - \Delta E_C \quad (7)$$

The conduction band offset $\Delta E_c$ at the AlGaN/GaN heterointerface is written [20]

$$\Delta E_C = 0.7[E_g^{AlGaN} - E_g^{GaN}] \quad (8)$$

The variation of band gap energy of the ternary AlGaN can be written as

$$E_g^{AlGaN} = xE_g^{AlN} + (1-x)E_g^{GaN} - 0.6x(1-x) \quad (9)$$

### *3.2 I–V model for AlGaN/GaN heterostructures based HEMT and MOSHEMT*

The analytical expression of the drain current is used for the sensitivity analysis and also calculated for AlGaN/GaN HEMT and MOSHEMT with and without biomolecules, can be formulated as [18]

$$I_d = \frac{W_g\mu_0\,C_{eff}}{L_g\delta}\left\{\sum_{i=0}^{6} k_i\,\left(\psi_{gd}^i - \psi_{gs}^i\right) + k_0 ln\frac{\psi_{gd}}{\psi_{gs}}\right\} \quad (10)$$

where $\mu_0$ represent the low field mobility. $W_g$ and $L_g$ are the width and the length of gate, respectively.

$$\psi_{gs} = \left(V_{gs} - V_{th} - V_s\right)^{1/3} + 2\theta, \psi_{gd} = \left(V_{gs} - V_{th} - V_{ds}\right)^{1/3} + 2\theta,$$

where $\delta = V_d - V_s/E_T L_g$ , $\theta = \lambda/3\,(C_{eff}/q)^{2/3}$ and $E_T$ is the critical field.

The expressions for the constants $k_i$ ($i = 1, \ldots, 6$) obtained during the integration of Eq. (10) are given in the Table I.

**Table 1** Expressions for constants terms obtained during the integration [21].

| Constants | Expressions |
|---|---|
| $k_0$ | $-288\theta^6$ |
| $k_1$ | $272\theta^5$ |
| $k_2$ | $-960\theta^4$ |
| $k_3$ | $200\theta^3$ |
| $k_4$ | $-70\theta^2$ |
| $k_5$ | $39\,\theta$ |
| $k_6$ | -3 |

### *3.3 Transconductance model for AlGaN/GaN heterostructures based HEMT and MOSHEMT*

An important parameter for estimating any device to evaluate its sensitivity performance [3] of the biosensor is the transconductance ($g_m$) which has a significant effect on drain current as it manifests as an amplification factor with $V_{ds} = const$, it can be defined as

$$g_m = \left.\frac{\partial I_{ds}}{\partial V_{gs}}\right|_{V_{ds}=const} \tag{11}$$

The transconductance can be extracted from Eq. (10) [21]

$$g_m = \frac{\mu_0 W_g C_{eff}}{\rho L_g}\left[\frac{1}{3(\psi_{gd}-2\theta)^2 - 3(\psi_{gs}-2\theta)^2}\right]\Omega_1 \tag{12}$$

where

$$\Omega_1 = \begin{bmatrix} \frac{288\theta^6}{(\psi_{gd}-\psi_{gs})} + 272\theta^5 + 1920\theta^4(\psi_{gd}-\psi_{gs}) + \\ 600\theta^3(\psi_{gd}-\psi_{gs})^2 \\ -280\theta^2(\psi_{gd}-\psi_{gs})^3 + 195\theta(\psi_{gd}-\psi_{gs})^4 - \\ 18(\psi_{gd}-\psi_{gs})^5 \end{bmatrix}. \tag{12a}$$

### *3.4 C-V Characteristics model for AlGaN/GaN heterostructures based HEMT and MOSHEMT*

The gate capacitances $C_{gs}$ and $C_{gd}$ can be expressed as $C_{gs} = \partial Q_g/\partial V_{gs}$ and $C_{gd} = \partial Q_g/\partial V_{ds}$[10].

The source capacitance can be expressed as [21]

$$C_{gs} = \frac{\mu_0 (qW_g\rho)^2}{I_{ds}}\left(\psi_{gd}^{1/3} - \psi_{gs}^{1/3}\right)\left(\frac{g_m}{I_{ds}} - 1\right) - \frac{qW\rho}{E_T}V_{ds} - \frac{L_g g_m}{\mu_0 E_T} \tag{13}$$

The drain capacitance can be expressed as [18]

$$C_{gd} = \frac{\mu_0 (qW_g\rho)^2}{I_{ds}}\left(\psi_{gd}^{1/3} - \psi_{gs}^{1/3}\right)\left(\frac{g_d}{I_{ds}} - 1\right) - \frac{qW\rho}{E_T}\psi_{gd} - \frac{L_g g_d}{\mu_0 E_T} \tag{14}$$

$$g_d = \frac{\mu_0 W_g C_{eff}}{\rho L_g}\left[\frac{1}{3(\psi_{gd}-2\theta)^2}\right]\Omega_1 \quad (15)$$

### *3.5 Sensitivity parameter expression*

The sensitivity parameter $S_{I_{off}}$ of the device at $V_{gs} = 0\ V$ can be defined by drain current and threshold voltage. For drain current, sensitivity parameter is defined as follows [22]

$$S_{I_{off}} = \frac{I_{off}\ (With\ Biomolecule\ Species)}{I_{off}\ (Without\ Biomolecule\ Species)} \quad \text{at } V_{gs} = 0\ V \quad (16)$$

The physical model parameters data used in numerical simulations are enlisted in Table 2.

**Table 2** List of physical model parameters used in numerical simulations.

| Parameters | Quantities | Value | Unit | Ref. |
|---|---|---|---|---|
| $E_T$ | Critical electric field | $178 \times 10^5$ | $V/m$ | [3] |
| $N_D$ | Doping concentration | $1.5 \times 10^{16}$ | $m^{-3}$ | [3] |
| $\phi_M$ | Metal work function | 4.5 | $eV$ | [3] |
| $\phi_0$ | Natural level Potential | 1.2 | $eV$ | [3] |
| $\mu_0$ | Low field mobility | 0.06 | $m^2/Vs$ | [3] |
| $\gamma_0$ | Fitting parameter | $4.12 \times 10^{-12}$ | $Vcm^{4/3}$ | [23] |

## 4. RESULTS AND DISCUSSION

In this section, we have discussed the validation of analytical model with numerical simulation results in terms of drain current, transconductance, and sensitivity parameter. We have compared also the performance between AlGaN/GaN HEMT and MOSHEMT device. The various of the biomolecule permittivity using in this work are listed in Table 3, the physical parameters values used for calculations are summarized in Table 4.

**Table 3** Permittivity of biomolecules [24,25]

| Biomolecules | Permittivity |
|---|---|
| ChOx | 3.3 |
| Protein | 2.5 |
| Streptavidin | 2.1 |
| Uricase | 1.54 |

**Table 4** Physical parameters and device details used for numerical simulation.

| Parameters | Quantities | Fig 3a [26] Sample 1 | Fig 3b [27] Sample 2 | Fig 4, 5 and 6 Our Model |
|---|---|---|---|---|
| $x\ (\%)$ | Al mole fraction | 15 | 20 | 30 |
| $\varepsilon_{ox}(F/m^2)$ | Oxide permittivity | --- | 9.1 $\varepsilon_0$ | 9.1 $\varepsilon_0$ |
| $\sigma_{pol}\ (m^{-2})$ | Spontaneous polarization charge | $1.15 \times 10^{17}$ [19] | $1.7 \times 10^{17}$ [19] | $1.55 \times 10^{17}$ [19] |
| $d_{AlGaN}(nm)$ | Barrier thickness | 22 | 30 | 15 |
| $L_g(\mu m)$ | Gate length | 1 | 1 | 0.3 |
| $W_g(\mu m)$ | Gate width | 75 | 100 | 100 |
| $d_{ox}\ (nm)$ | Oxide thickness | --- | 16 | 10 |

Figure 3(a) and Figure 3(b) show a comparison of the output characteristics predicted by the model with the experimental data for the AlGaN/GaN heterostructures based HEMT and MOSHEMT devices. It is clear that the numerical simulation results of the analytical model are in good agreement with experimental data extracted from [26] and [27], respectively. Besides, to validate the numerical simulation results of the analytical model exactly the same dimensions of AlGaN/GaN heterostructures based HEMT and MOSHEMT devices are considered from experimental data. Moreover, the device simulation MATLAB calculations for the sample 1 and sample 2 as depicted in Figure 3.

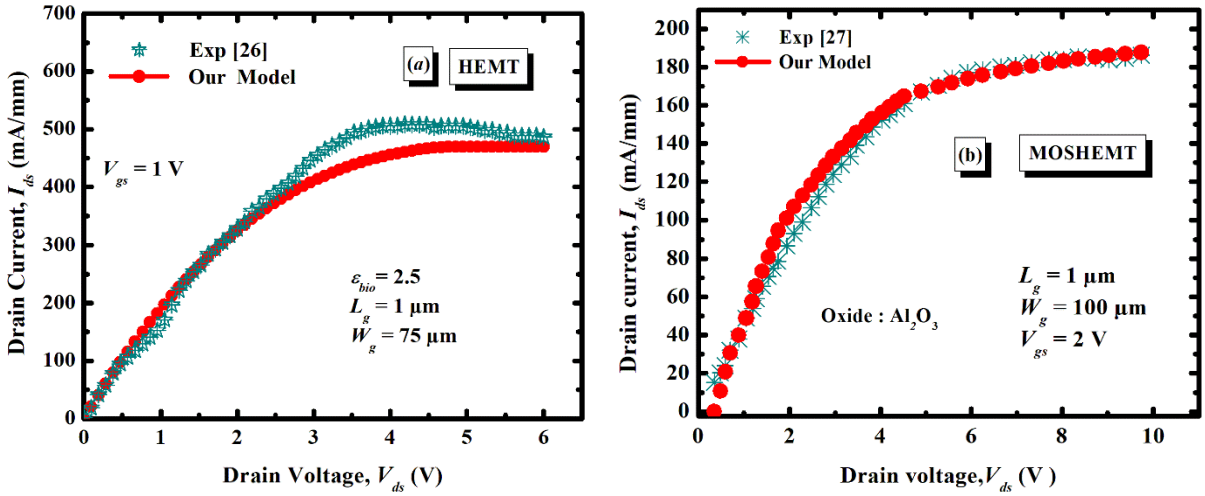


**Figure 3.** Comparison of the *I-V* output characteristics. (a) AlGaN/GaN HEMT and (b) AlGaN/GaN MOSHEMT structure with experimental data have been taken from [26] and [27], respectively.

Figure 4(a) and 4(b) shows a comparison of the output characteristics of analytical models of AlGaN/GaN HEMT and MOSHEMT devices with and without biomolecule, these models are simulated with Atlas-TCAD that present the results which are in good agreement with each other.

When the biomolecule of the protein permittivity ($\varepsilon_{bio} = 2.5$) is introduced in the cavity region of the biosensor, there is improvement in the carrier concentration in the channel region which causes change in the drain current, that present the AlGaN/GaN heterostructures based HEMT and MOSHEMT devices which are in good performance for biosensing applications.

For the both device the gate biasing varies from (0 V to 14 V). As seen, that in the case of AlGaN/GaN HEMT the variation of drain current is substantially higher than AlGaN/GaN MOSHEMT at the gate voltage of 0V in which the variation of drain current is limited to 75.07 mA/mm in case of AlGaN/GaN MOSHEMT. Thus, in contrast the variation of drain current of AlGaN/GaN HEMT is 244.42 mA/mm.

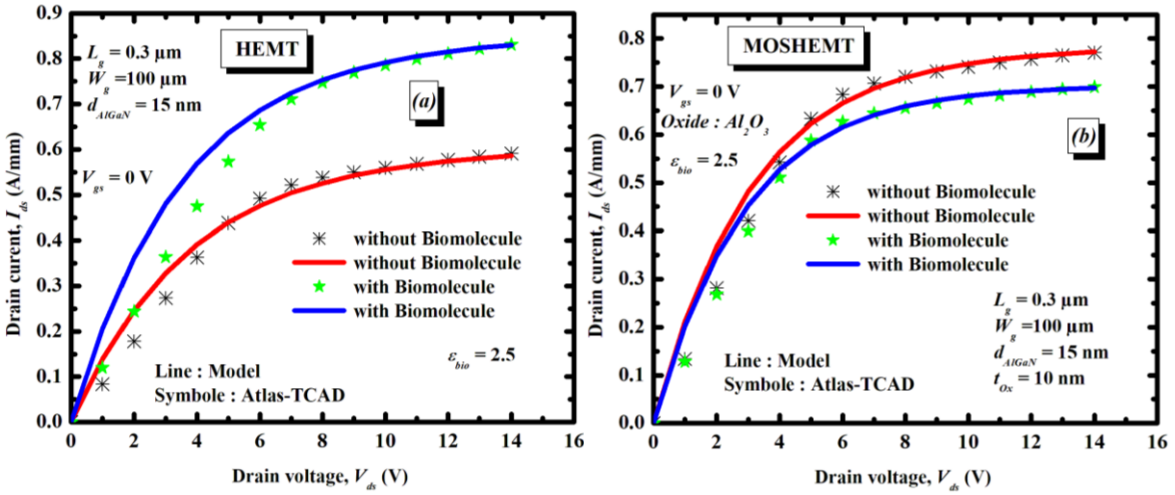


**Figure 4.** Comparison of the current-votltage characteristics. (a) AlGaN/GaN heterostructures based HEMT and (b) AlGaN/GaN heterostructures based MOSHEMT.

The transfer characteristics of AlGaN/GaN heterostructures based HEMT and MOSHEMT with and without biomolecule are plotted in Figure 5(a) and 5(b).

When the biomolecule is introduced in to the cavity region, it can be seen there is a variation in the drain current. The variation in drain current for the transfer characteristics can also be considered as one of the sensing parameters for biomolecules detection. It is here observed in case of AlGaN/GaN heterostructures based HEMT the variation of drain current is substantially higher than AlGaN/GaN MOSHEMT at the Drain voltage of 5 V, in which the variation of drain current is limited to 86.88 mA/mm in case of AlGaN/GaN heterostructures based MOSHEMT, in contrast the variation of drain current of AlGaN/GaN HEMT is 542.27 mA/mm.

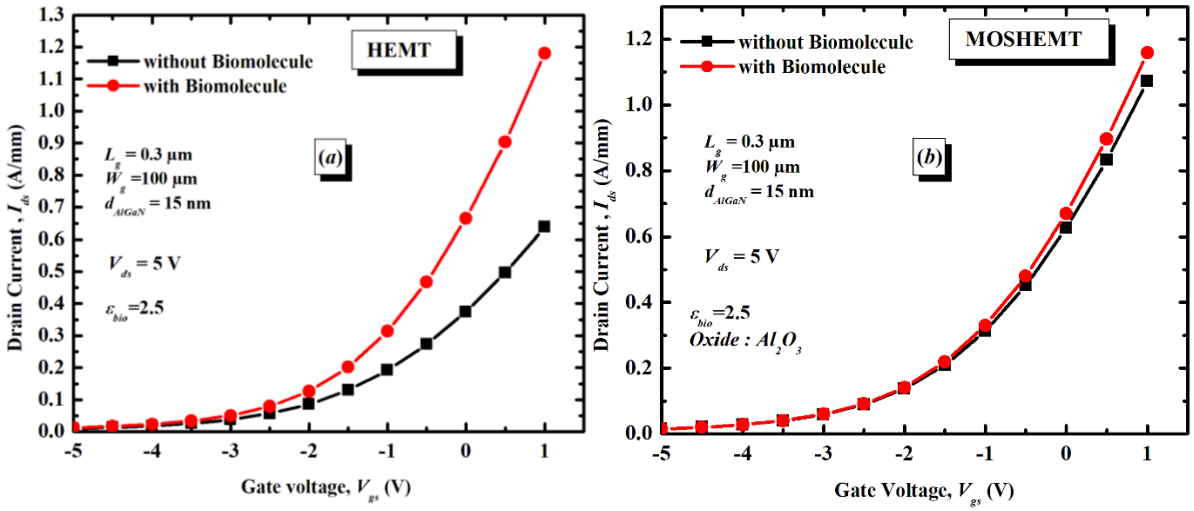


**Figure 5.** Comparison of the modeled $I_{ds}$–$V_{gs}$ characteristics, (a) AlGaN/GaN heterostructures based HEMT and (b) AlGaN/GaN heterostructures based MOSHEMT.

Moreover, the transconductance of AlGaN/GaN heterostructures based HEMT and MOSHEMT devices with and without biomolecule are depicted in Figure 6(a) and 6(b). Besides, the transconductance of a device depends on $V_{th}$, the value of this $V_{th}$ changes when the biomolecule is introduced into the cavity which thereby causing a change in transconductance ($g_m$).
Furthermore, when the biomolecule protein of the permittivity at 2.5 is introduced into the cavity, the transconductance ($g_m$) shows a remarkable difference value that can be used as a good sensing parameter. In addition, AlGaN/GaN heterostructures based HEMT device show higher variation of transconductance as compared with AlGaN/GaN MOSHEMT device as shown

in Figure 6(a) and 6(b) bellow. Thus, the variation of transconductance is limited to 44.84 mS/mm in case of AlGaN/GaN heterostructures based HEMT and in contrast that the variation of transconductance of AlGaN/GaN heterostructures based MOSHEMT is 20.89 mS/mm.

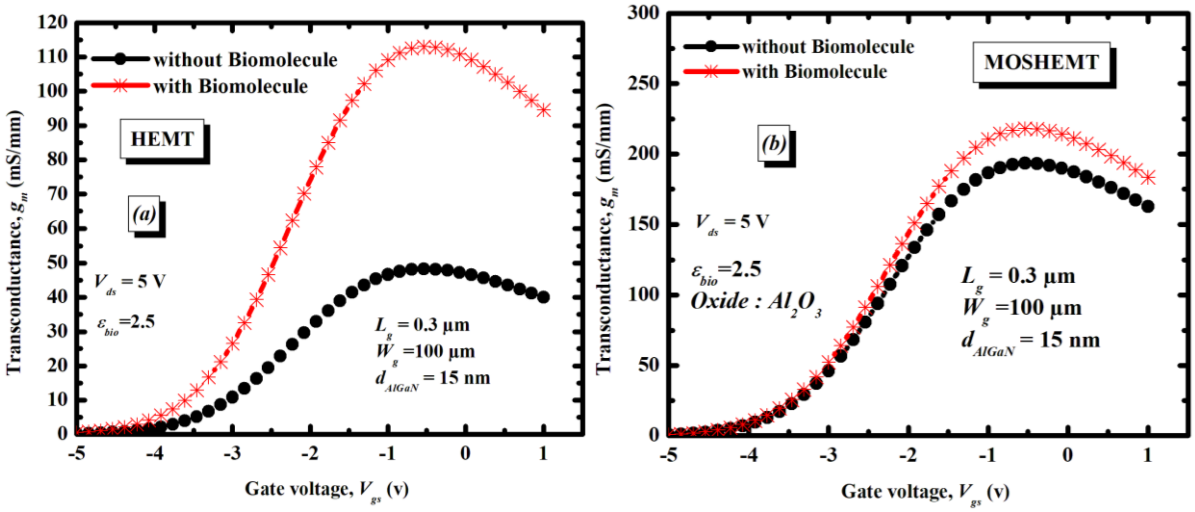


**Figure 6.** Comparison of the modeled transconductance. (a) AlGaN/GaN heterostructures based HEMT and (b) AlGaN/GaN heterostructures based MOSHEMT.

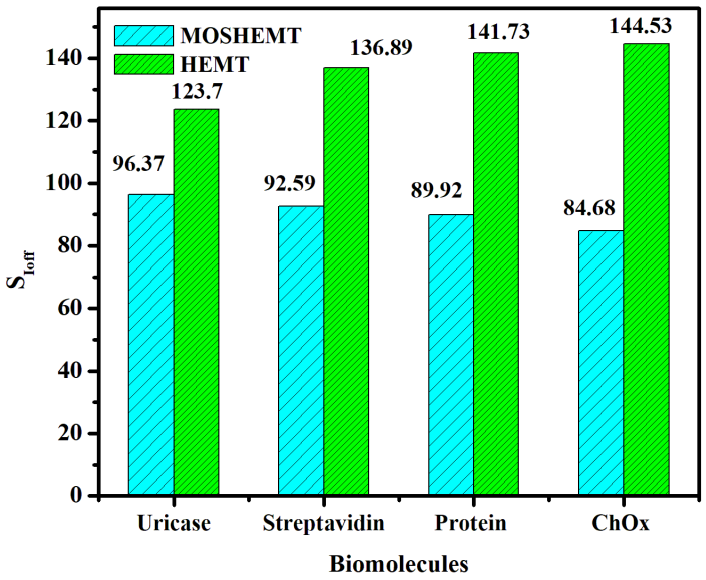


**Figure 7.** Comparison of the sensitivity ($I_{bio}/I_{air}$) for AlGaN/GaN heterostructures based HEMT and MOSHEMT.

Figure 7 shows a comparison of the effect of sensitivity parameter on the electrical performance of AlGaN/GaN HEMT and MOSHEMT devices with and without biomolecule. It is clearly seen that the sensitivity parameter $(S_{I_{off}})$ is much higher in the AlGaN/GaN HEMT case compared to the AlGaN/GaN MOSHEMT case. ChOx biomolecule presents highest sensitivity compared with all the biomolecules for AlGaN/GaN HEMT. As can be observed from Figure 7, when the value of the biomolecule permittivity increases, the sensitivity of the biosensor increases. For AlGaN/GaN MOSHEMT Uricase biomolecule shows highest sensitivity among all biomolecules, when the value of the biomolecule permittivity increases, the sensitivity of the biosensor decreases.

**Table 5** Comparative between AlGaN/GaN HEMT and MOSHEMT biosensors

| Device | $\Delta I_{on}$*(mA/mm) ($V_{ds}$ = 5 V) | $\Delta g_m$ (mS/mm) ($V_{ds}$ =5 V) | ($I_{bio}/I_{air}$) *100 ($\varepsilon_{bio} = 2.5$) |
|---|---|---|---|
| AlGaN/GaN HEMT (Our Model) | 542.27 | 44.84 | 141.73 |
| AlGaN/GaN MOSHEMT (Our Model) | 86.88 | 20.89 | 89.92 |

**Change in drain current = Drain current without Biomolecule – Drain current with Biomolecule.*

**Table 6** Comparison between our models, MOSHEMT [1] and GAA-JLT [22]

| Device | Change in current in drain current ($\Delta I_{on}$) (mA/mm) |
|---|---|
| AlGaN/GaN HEMT (This work) | 542.27 |
| AlGaN/GaN MOSHEMT (This work) | 86.88 |
| AlGaN/GaN MOSHEMT [1] | 136 |
| GAA-JLT ($\Delta I_{off}$) [21] | 0.0033 |

## 5. CONCLUSION

The simulation results of the analytical modeling for electrical properties of AlGaN/GaN heterostructures based HEMT and MOSHEMT with and without biomolecule were proposed and compared. A maximum drain current density variation and higher transconductance, were seen when the protein biomolecule is filled in the cavity region, it can be concluded that the HEMT and MOSHEMT devices proposed exhibit good performance for biosensing applications.

Besides, the simulation results obtained show that the AlGaN/GaN HEMT present a higher variation in drain current ($\Delta I_{on}$) and sensitivity for various biomolecules which is change in current of 542.27 mA/mm and 86.88 mA/mm, drain off sensitivity of 141.73 % and 89.92% at $\varepsilon_{bio} = 2.5$ have been obtained for AlGaN/GaN heterostructures based HEMT and MOSHEMT with proposed model, respectively. Thus, the electrical performance of AlGaN/GaN heterostructures based HEMT is higher than AlGaN/GaN heterostructures based MOSHEMT for biosensing applications.

The change in the maximum drain current observed by protein biomolecule is compared with the results of AlGaN/GaN heterostructures based MOSHEMT and GAA-JLT. Finally, the AlGaN/GaN heterostructures HEMT biosensors presented higher performance offered higher performance.

## REFERENCES

[1] H. M. Shaveta, A.Maali and C. Rishu. J Mater Sci: Mater Electron, vol **31,** (2020) pp.16609–16615.
[2] Z. Gu, J. Wang, B. Miao, L. Zhao, X. Liu, D. Wu, and J. Li. RSC Advance, vol **9,** (2019) pp. 15341–15349.
[3] S.N. Mishra, R. Saha, and K. Jena. ECS J. Solid State Sci. Technol. vol **9,** (2020) pp. 1-15.
[4] S.J. Pearton, B. S. Kang, S. Kim, F. Ren, B. P. Gila, C. R. Abernathy, J. Lin and S. N. G. Chu. J. Phys*:* Condens. Matter, vol **16**, (2004) pp. R961–R994.
[5] A. Varghese, C. Periasamy, L. Bhargava. IEEE Trans. Nanotechnol, vol **18**, (2019) pp. 747–755.
[6] A. Koudymov, H. Fatima, G. Simin, J. Yang, M. Asif Khan, A. Tarakji, X. Hu, M. S. Shur, and R. Gaska. Appl. Phys. Lett, vol **80** (2002) pp. 3216-3218.

[7] M. Asif Khan, X. Hu, G. Sumin, A. Lunev, J. Yang, R. Gaska, and M. S. Shur. IEEE Elec. Dev. Letters, vol **21** (2000) pp. 63–65.
[8] B. S. Kang, H. T. Wang, T. P. Lele, Y. Tseng, F. Ren, S. J. Pearton, J. W. Johnson, P. Rajagopal, J. C. Roberts, E. L. Piner and K. J. Linthicum. Appl. Phys. Lett, vol **91** (2007) pp. 112106-1–112106-3.
[9] J. Cheng, J. Li, B. Miao, J. Wang, Z. Wu, D. Wu, and R. Pei. Appl. Phys. Lett, vol **105,** (2014) pp. 083121-1–083121-4.
[10] S.U. Schwarz, S. Linkohr, P. Lorenz, S. Krischok, T. Nakamura, V. Cimalla, C. E. Nebel, and Oliver Ambacher. Phys. Status Solidi A, vol **208**, (2011) pp. 1626–1629.
[11] N. Kazanskaya, A. Kukhtin, M. Manenkova, N. Reshetilov, L. Yarysheva, O. Arzhakova, A. Volynskii and N. Bakeyev. Biosens. Bioelectron, vol **11**, (1996) pp. 253–261.
[12] K. H. Chen, B. S. Kang, H. T. Wang, T. P. Lele, F. Ren1, Y. L. Wang, C. Y. Chang, S. J. Pearton, D. M. Dennis, J. W. Johnson, P. Rajagopal, J. C. Roberts, E. L. Piner, and K. J. Linthicum. Appl. Phys. Lett. Vol **92**, (2008) pp. 192103-1–192103-3.
[13] Y. Chen, R. Ren, H. Pu, X. Guo, J. Chang, G. Zhou, S. Mao, M. Kron, J. Chen. Sci. Rep, vol **7,** (2017) pp. 1–8.
[14] G. Seo, G. Lee, J.-O. Lee, B.T. Kim, E.C. Park, S.I. Kim Am. Chem. Soc. Vol **14**, (2020) pp. 5135–5142.
[15] Aasif Mohammad Bhat, Nawaz Shafi, Chitrakant Sahu and C.Periasamy. IEEE Sensors Journal, vol **18**, (2021) pp. 19753-19761.
[16] Ritu Poonia, Aasif Mohammad Bhat, C. Periasamy, Chitrakant Sahu. Silicon, (2022) pp. 1-14.
[17] Aasif Mohammad Bhat, Arathy Varghese, Nawaz Shafi and C. Periasamy. IETE Journal of Research, (2022) pp. 1-10.
[18] S.N. Mishra and K. Jena. Journal of the Korean Physical Society, vol **74**, (2019) pp. 349–357.
[19] O. Ambacher, J. Smart, J. R. Shealy, N.G. Weimann, K. Chu, M. Murphy, W.J. Schaff, L.F. Eastman, R. Dimitrov, L. Wittmer, M. Stutzmann, W. Rieger, and J. Hilsenbeck. J. App. Phy. vol **85**, (1999) pp. 3222–3233.
[20] P. Gangwani, S. Pandey, S. Haldar, M. Gupta, and R. S. Gupta. Solid-State Electron. vol **51**, (2007) pp. 130–135.
[21] K. Jena, R. Swain, and T.R. Lenka. IET Circuits Devices Syst, vol **10**, (2016) 423–432.
[22] Y. Pratap, M. Kumar, S. Kabra, S. Haldar, R.S. Gupta, M. Gupta. J Comput Electron, vol **17**, (2118) pp. 288–296.
[23] S. Baskaran, A. Mohanbabu, N. Anbuselvan, N. Mohankumar, D. Godwinraj, C.K. Sarkar. Superlattices and Microstructures. vol **64**, (2013) pp. 470–482.
[24] P. Dwivedi and A. Kranti. IEEE Sensors J. vol **17**, (2017) pp. 1030–1036.
[25] A. Varghese, C. Periasamy, and L. Bhargava. IEEE Sens. J. vol **18** (2018) pp. 9595–9602.
[26] Y.F. Wu, S. Keller, P. Kozodoy, B.P Keller, P Parikh, D. Kapolnek, S.P. Denbaars, U.K. Mishra. IEEE Electron Dev Lett. vol **18**, (1997) pp. 290–292.
[27] W. D. Hu, X. S. Chen, Z. J. Quan, X. M. Zhang, Y. Huang, C. S. Xia, W. Lu, and P. D. Ye. J. Appl. Phys. vol **102**, (2007) pp. 034502.